J Solid State Electrochem (2007) 11:1085–1092
DOI 10.1007/s10008-006-0242-8

ORIGINAL PAPER

Theoretical analysis of the performance of a model supercapacitor consisting of metal oxide nano-particles

Hossein Farsi · Fereydoon Gobal

Received: 12 September 2006 / Revised: 23 October 2006 / Accepted: 3 November 2006 / Published online: 5 December 2006

Abstract The factors influencing the electrochemical behaviour of a supercapacitor have been partly examined in this work. The effects of so-called intrinsic parameters, i.e. exchange current density, unit cell length and double layer (DL) capacitance; as well as the so-called application parameters, i.e. cell current, on the cell potential discharge time have been considered. The contributions of each type of capacitors, DL capacitor and faradaic supercapacitor under various states of operation and material have been analyzed, and the competing (compensating) effects of the two types of capacitors as regards to the discharge and power characteristics manifested by current–potential and energy–power (Ragone plots) are elucidated.

Keywords Supercapacitor · Ragone plot · Discharge curve · Double layer current · Faradaic current · Metal oxide nano-particles

Introduction

Electrochemical capacitors are of considerable demand, where high power and energy density as well as reliabilities [1–4] are requested, and can be divided in two categories, those based on the energy stored in double layer (DL) structure and those that rely on the faradaic reactions at the interfaces. The latter often involves not only charge transfer but also surface reactions and mass transfer processes.

Activated carbon having specific surface area in the order of 10^3 m^2g^{-1} form typical DL capacitors [5], whereas high surface area amorphous hydrated oxide of RuO_2 [6, 7], NiO [8, 9], CoO_x [9, 10], MnO_x [11], etc. are of potential use in faradaic and mixed capacitors. Many models have been developed to account for the effects of various variables on the performance of both types of capacitors where both charge and discharge cycles have been considered. The studies encompass a broad range of variables, modes of operation, materials, etc. Chuan Lin et al. [12] have developed an elaborate model to simulate the behaviour of a $RuO_2.xH_2O$ based capacitor under galvanostatic regime, whereas both DL and faradaic processes have been taken into account. The favourable effect of decreasing the particle size on the performance, as well as that of the faradaic process, in enhancing the power and energy density has been reported. On the other hand, Changqing Lin et al. [13] have used a model in the context of the dilute solution theory to investigate the effect of carbon content and discharge current density on the performance of capacitors developed by dispersing RuO_2 within the pores of active carbon. They concluded that large current densities hamper the utilization of stored charge, and large pore samples are, thus, favoured. Also, they report that increasing carbon content deteriorates the delivered charge and energy density, but the reductions were not severe. In most studies relevant to the performance of energy storage devices, Ragone plots that relate the energies accessible at various power output of the device have been employed [4]. The theory and usefulness of Ragone plots have been recently reviewed by Christen et al. [14, 15]. We have employed the method of artificial neural network to

H. Farsi (✉) · F. Gobal
Department of Chemistry, Sharif University of Technology,
P.O. Box 11365-9516, Tehran, Iran
e-mail: farsi@mehr.sharif.edu

F. Gobal
e-mail: gobal@sharif.edu

predict the electrical output of a supercapacitor on the basis of the electrochemical and geometrical characteristics of its constituent electroactive materials [16]. We have had some success with both the predictions and rationalization of the behaviour in limited domains of studies. This type of study, although of excellent predictive power, does not reveal how any one of the input parameters (say the exchange current density of the electrode process) affects any one of the outputs (say power output) under other specified conditions.

The purpose of the present work is to investigate the effects of the exchange current density, lengths of unit cells and discharge current on the discharge characterizations of a model supercapacitor (DL+faradaic capacitor) as exemplified by the galvanostatic discharge curves and also the Ragone plots.

Materials and methods

We have basically employed the model proposed by Lin et al. [12] where two identical $RuO_2.xH_2O$ electrodes separated by an ionic conducting separator are considered. The electrolyte, H_2SO_4, is assumed to completely fill the pore structure of the electrodes. The details of the model can be found in the original literature [12], and in this study, only the equations dominating our calculations are reproduced. The faradaic current, j_f, is given by the Butler–Volmer equation:

$$j_f = i_0[\exp(\alpha_a f(E-U_1)) - \exp(-\alpha_c f(E-U_1))], \quad (1)$$

where i_0 is the exchange current density, $f = \frac{F}{RT}$ with the symbols have their usual meaning, α_a and α_c are the anodic and cathodic transfer coefficients that, in this work, are taken as 0.5. E is the local electrode potential, and U_1 is the equilibrium potential both in units of volts. U_1 depends on the fraction of the amount of electrocative material in its oxidized state, θ, that in turn, is linearly related to the state of charge, δ, (of the capacitor's electrode) through $\delta=0.5\theta$ [7, 12]. On the other hand, θ is related to more easily measurable quantities through

$$\frac{d\theta}{dt} = \frac{S_V j_f}{(Q_{f,ox} - Q_{f,red})}, \quad (2)$$

with S_V being the specific area (area per unit volume of material) with its magnitude given by

$$S_V = \frac{6(1-\varepsilon)}{d} \quad (3)$$

It has been assumed that the electrode is composed of spherical nano-particles of active ingredient of dimension d, and the porosity of the electrode ε is assumed to be 0.25. In Eq. (3), $Q_{f,ox}$ and $Q_{f,red}$ are the faradaic charges per unit volume of the electrode in the fully oxidized and reduced states with

$$Q_{f,ox} = \frac{S_V \delta F}{h^2 L_A}, \quad (4)$$

where L_A is the Avogadro's number, h is the length of unit cell on the surface (taken 0.4 nm for RuO_2 [17]) and δ is the state of charge equal to 0.5 for the fully charged electrode. The faradaic charge per unit volume of fully reduced electrode, $Q_{f,red}$, is taken as zero. Finally, the local potential, E, at various points along the depth of the electrode is given through

$$\frac{\partial^2 E}{\partial \xi^2} = \tau \frac{\partial E}{\partial t} + \tau \frac{j_f}{C_{dl}} \quad (5)$$

with $C_{dl} = 2 \times 10^{-5}\,\mathrm{F\,cm^{-2}}$, $\xi = \frac{x}{L}$ (fractional distance through the electrode), and τ DL time constant is

$$\tau = S_V C_{dl} L^2 \left(\frac{1}{\sigma} + \frac{1}{k_p}\right), \quad (6)$$

with σ and K_p being the electrode (active ingredient) and the electrolyte conductivities with the values of 1×10^5 S cm^{-1} [18] and 0.1 S cm^{-1} [12], respectively.

We have employed backward finite difference method through Band(J) algorithm [19] in Matlab environment and linearized the exponential term basically similar to the method used by Lin et al. [12]. One hundred and three space and 4,001 time slots have been used, and it was observed that no further improvements (smoothness) were observed upon any increase in the number of space and time slots. Following the calculations of E and θ, the values of DL as well as the faradaic current have been calculated through

$$i_c = -S_V C_{dl}\left(\frac{\partial E}{\partial t}\right) \quad (7)$$

$$i_f = -S_V j_f \quad (8)$$

The dimensionless cell potential, Φ_{cell}, has also been calculated through [13]

$$\Phi_{\mathrm{cell}} = 2\left[E|_{\xi=0} - V_0\right] - 2\left[\phi_2|_{\xi=1} - \phi_2|_{\xi=0}\right] - \frac{I_{cell} L_s}{E_0 k_s}, \quad (9)$$

where ϕ_2 is the dimensionless potential in the electrolyte phase; E_0 is the local potential at $t=0$ and is set at $2v_0$ volt with v_0, initial potential, equal to 0.5 for the case of RuO_2 [7]; V_0 is the dimensionless initial equilibrium potential prior to charging and is taken 0.5; E' is the dimensionless localized potential; L_s and k_s are the thickness of the

separator and the conductivity of the solution inside of the separator pores. All dimensionless potential terms are calculated by dividing the potential terms by E_0, and all the cell characteristics are calculated at $\xi=1$ (on the electrode surface) and at t_d (discharge time).

Results and discussions

The effect of unit cell length

Under galvanostatic discharge regime and for the electrode comprising of 5-nm-sized nano-particles having $i_0 = 1 \times 10^{-5}\,\mathrm{A\,cm^{-2}}$ (this value has been considered for RuO_2 by Lin et al.), the discharge characteristic of the capacitor, as influenced by various unit cell length (including 0.4 nm for RuO_2) of the electroactive material at cell current in the range of 0.1 to 5.0 A, have been studied. The results are presented in Fig. 1. The appearance of the slope change in the cell potential vs. discharge time (t_d) is interesting, and it is more pronounced at smaller unit cell lengths, and under a higher discharge rate. To rationalize the findings, it seems that, in a sense, the smallest h values reflects the highest amount of change available per unit area of the surface, as the amount of the active material will be the highest. In this work, we have employed t_d as the capacity criteria and not the relative utilization [20], $t^*i^*_{cell}$ to be able to make real time judgment concerning the effect of i_0 and h. In fact, keeping the nano-particle size, d, constant (as done in this work) makes the two criteria equivalent. As for the slope change, in the early stages of discharge and especially under high currents, electrochemistry cannot provide the energy drawn from the cell and an energy (potential) barrier; its height is proportional both to the cell current and

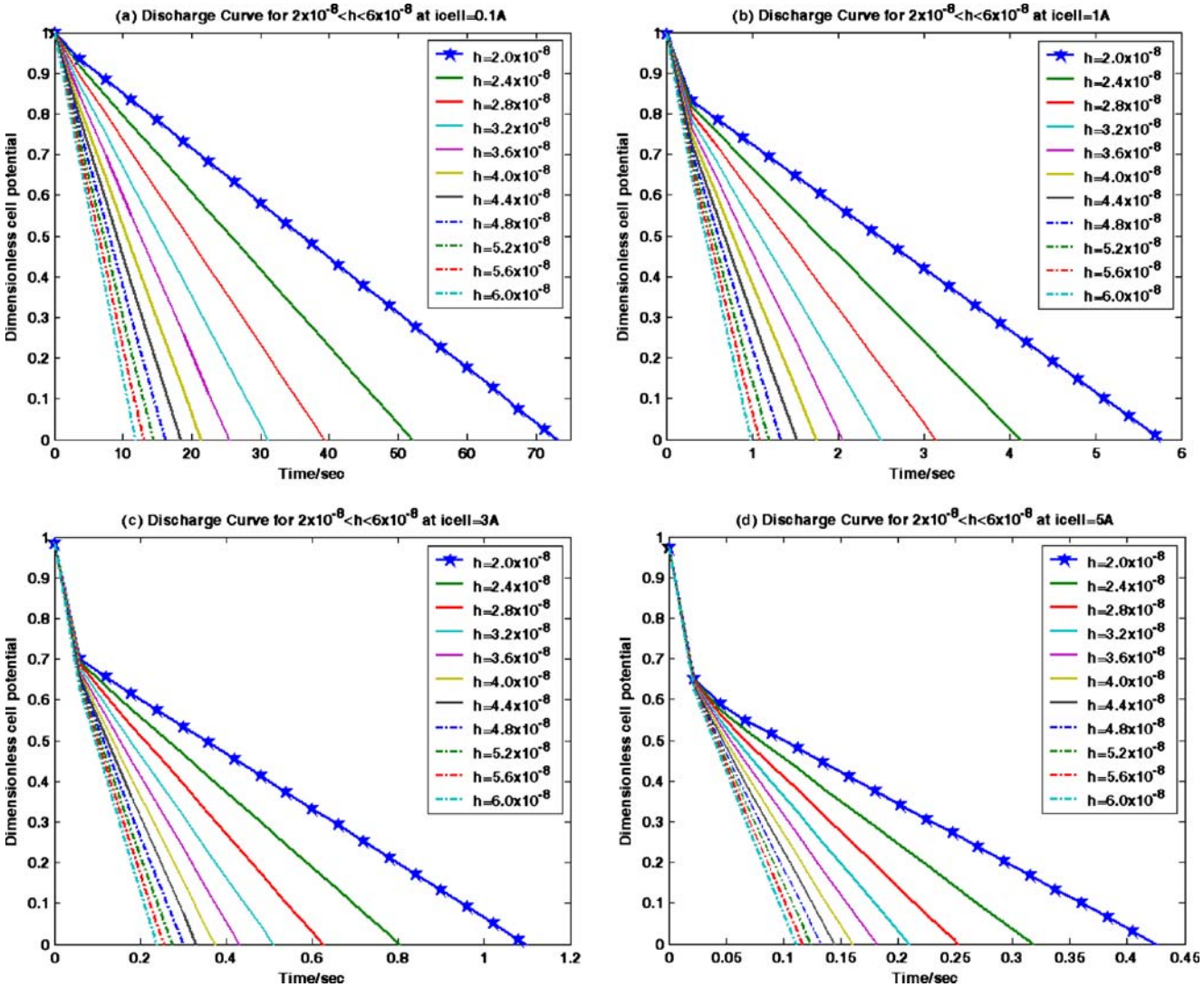

Fig. 1 Galvanostatic discharge curve for simulated electrodes with 5 nm nano-particles having and different unit cell length in i_{cell}=0.1 A (**a**), 1.0 A (**b**), 3.0 A (**c**) and 5.0 A (**d**)

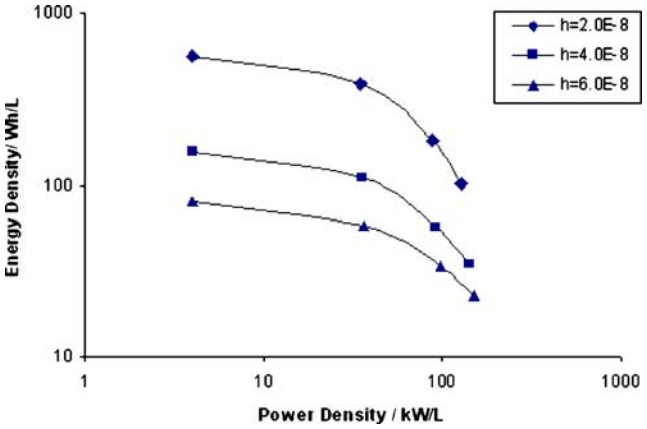

Fig. 2 Ragone plot for simulated supercapacitors with 5-nm nano-particles having with three values of h presented at the legend

the number of electrochemically active sites (inverse of h must be overcome). This gives rise to a sharp drop of cell potential at the early stages of discharge. From another point of view, electrochemistry lags behind, and DL capacitor somewhat takes control in this region. Comparing the utility of two cells with h values of 2×10^{-8} and 6×10^{-8} cm discharged at two cell currents of 1 and 0.1 A, the energy drops at 21 and 16%, respectively, pointing to the ease of discharge as h is decreased. This point will be further addressed using Ragone plots.

Figure 2 presents the Ragone plots for capacitors with different h values. The Ragone plots reflect the energy and power density relations as defined through Eqs. (10) and (11):

$$\text{Energy density} = \frac{i_{\text{cell}}\Phi_{\text{ave}}t_{\text{d}}}{V_{\text{cell}}} \tag{10}$$

$$\text{Power density} = \frac{i_{\text{cell}}\Phi_{\text{ave}}}{V_{\text{cell}}} \tag{11}$$

with Φ_{ave} as the average cell potential along t_d and V_{cell} as the cell (here capacitor) volume. In this pattern, the slowly decreasing energy density is terminated to a significantly sharper decreasing dependency. The interpretation of the findings basically follows the preceding discussion and is based on the contributors of faradaic processes, which are slow and encounter kinetic barrier and the DL discharge that is fast. Systems having small h values provide higher

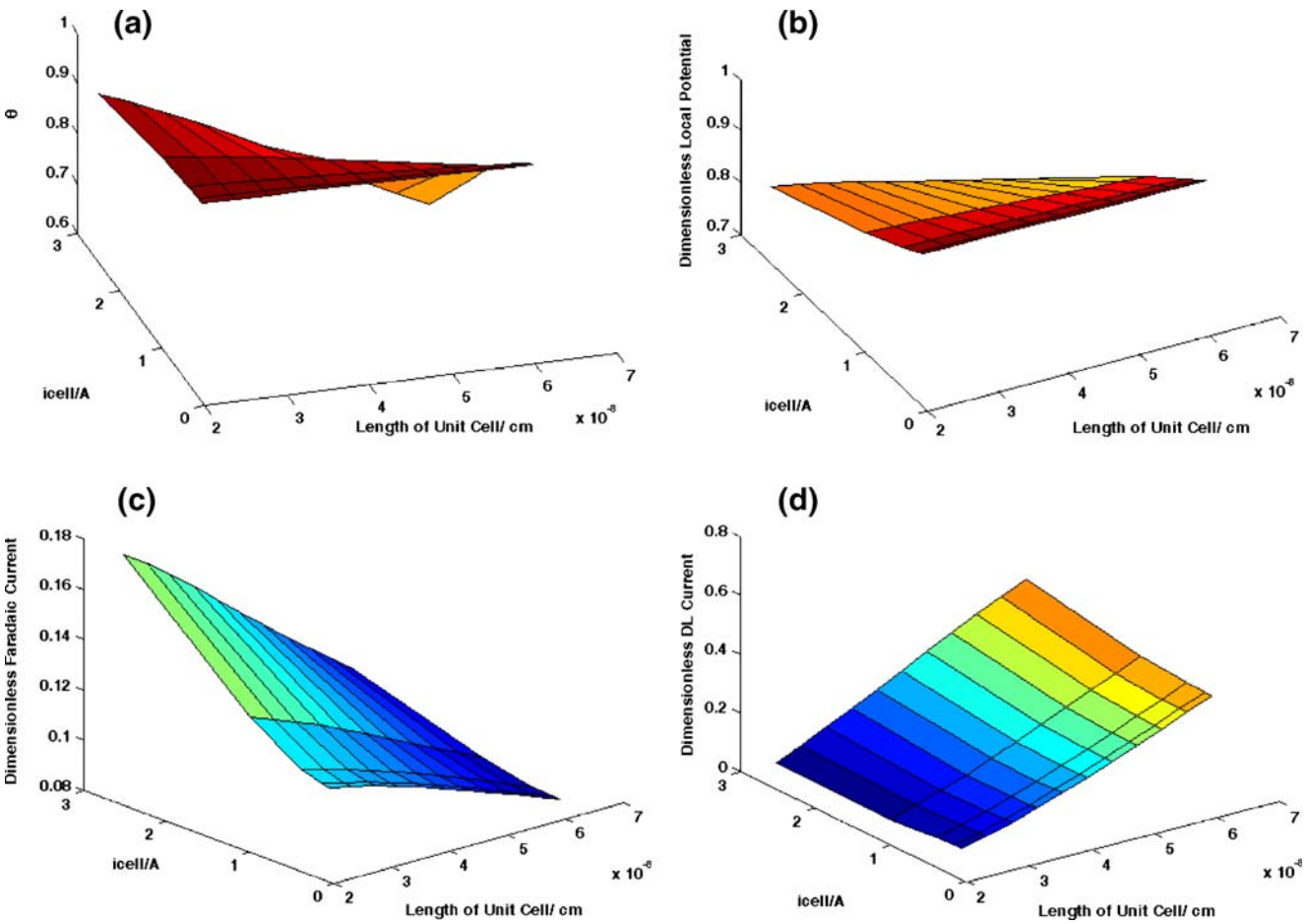

Fig. 3 Dependency of θ, E, faradaic and DL current to the i_{cell} and the length of unit cell for simulated electrodes with 50-nm nano-particles having $i_0 = 1 \times 10^{-5}\,\text{A cm}^{-2}$

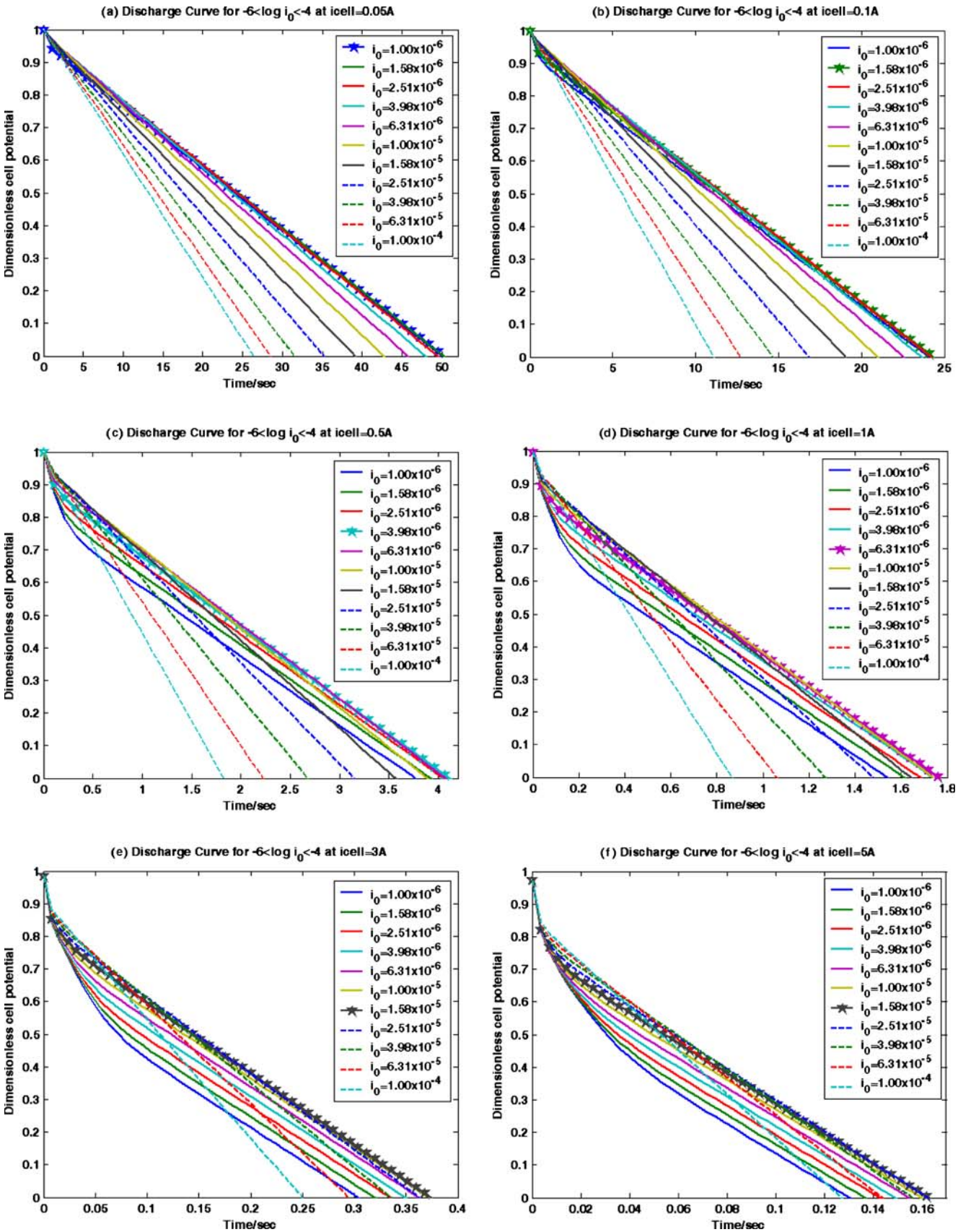

Fig. 4 Galvanostatic discharge curve for simulated electrodes with 5-nm nano-particles having and different surface exchange current density in i_{cell}=0.05 A (**a**), 0.1 A (**b**), 0.5 A (**c**), 1.0 A (**d**), 3.0 A (**e**) and 5.0 A (**f**)

energy densities that are, in turn, more susceptible to discharge at higher power densities that are a consequence of the fast discharge of large amounts of charge. The high energy densities accessible at low powers are provided by the faradaic process with kinetic barriers, whereas at higher powers, energy density drops sharply, and the drop is more pronounced with more facile systems, high i_0 and low h values. This is in accord with the simulation findings.

Figure 3a presents the variation of θ with i_{cell} and h in a three-dimensional representation. Although at low cell current and low h values θ is not significantly influenced by either (plenty of oxidized sites with a small rate of discharge), the dependency is more pronounced at a high value of both. Large i_{cell} and h values correspond to the fast removal of low levels of charge that signifies low θ values. Figure 3b presents the changes of dimensionless potential at the surface of the active material against i_{cell} and h, where dramatic changes at high values of both quantities have been observed. Although this, in principle, follows θ behaviour, the attenuation is much smaller, and we attribute it to both faradaic and DL contributors. Figure 3c,d presents the faradaic and DL contribution of the discharge current, varied according to the selection of cell current and h. The planes run in principle in opposite directions due to the compensating nature of the two processes in providing the cell current. Interestingly, at low h values, the drawn high cell current mostly comes from the faradaic process, whereas DL discharge take over at higher h values in excellent agreement with expectations. In fact, the summation of i_c and i_f allocates a portion of i_{cell} that increases with the increase in i_{cell}. The effects of h, as reflected in the number of active sites per unit area of the electroactive materials, have been experimentally addressed by Doubova et al. [21], where the electrochemical activities of various crystallographic planes of RuO_2 having different h values have been studied. Our results are in qualitative agreement with the experimental findings.

The effect of exchange current density

Figure 4 presents the discharge characteristic of a simulated supercapacitor signified as cell potential drop with respect to the time (discharge time) measured at different i_{cell} values in the range of 0.05 to 5.0 A for various values of i_0. No monotonic behaviour has been observed. Whereas at discharge current density of 0.1 A, the highest available capacity occurs at $i_0 = 1.58 \times 10^{-6}$ A cm^{-2}; at 3 A discharge current, it corresponds to 1.58×10^{-5} A cm^{-2}. Apparently the point (in fact region) of slope change shifts as the value of i_0 is scanned at different discharge currents. The behaviour has its roots in how the kinetics of the discharge process copes with the imposed cell current. To clarify the situation, plots of t_d (at $\Phi_{cell}=0$) vs. i_0 have been constructed at various i_{cell} values, Fig. 5. A sharp rise followed by a slow decline has been witnessed. Passing through a point of maximum is the result of competition of two processes, one that consumes electron, i_{cell}, and the one that is responsible for providing electrons, i_0. If the rate of supply is fast, large i_0, the discharge time is small. Similarly when i_0 is too small, the system does not respond to cell current and is in the state of "virtual discharge" (minute amount of charge quickly disappears). Obviously, the

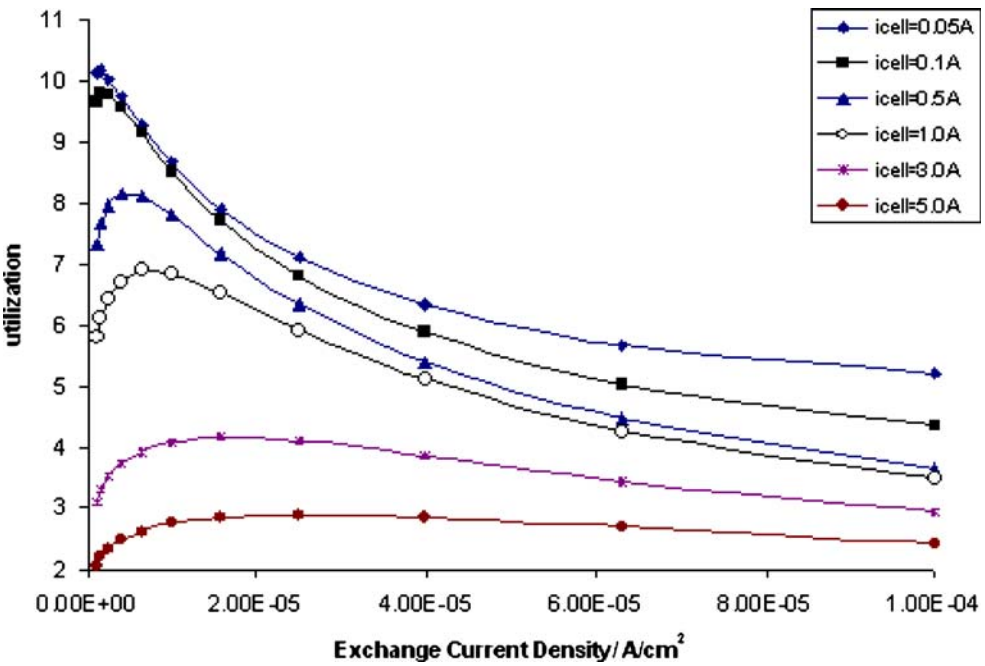

Fig. 5 Utilization vs. exchange current density for simulated supercapacitors having 5-nm nano-particles and unit cell length equal to 0.4 nm. Note that t_d is a criterion of utilization

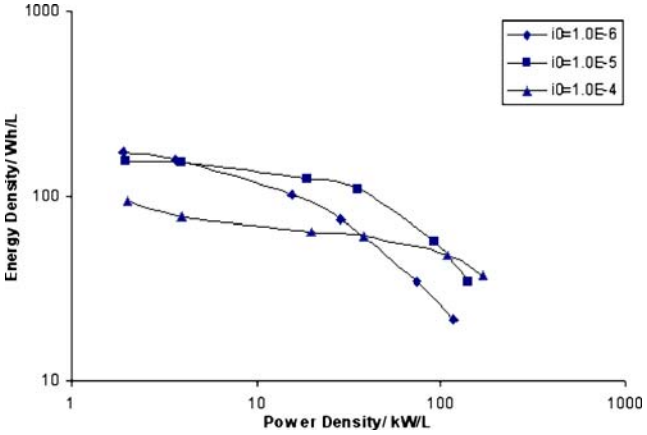

Fig. 6 Ragone plot for simulated supercapacitors having 5-nm nano-particles and h=0.4 nm with three different values of i_0 presented at the legend

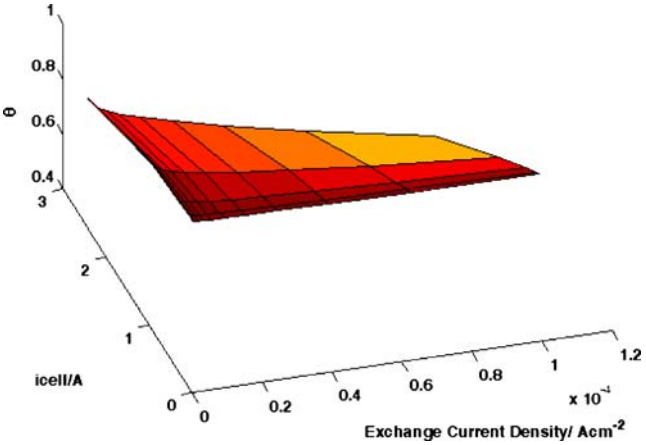

Fig. 8 Dependency of θ to i_{cell} and exchange current density for simulated electrodes having 5-nm nano-particles and h=0.4 nm

system should go through a maximum as i_0 is raised. Our predictions are in qualitative agreement with the existing literature [22, 23].

Figure 6 presents the Ragone plot at different i_0 values. Dramatic early drop in the energy density accompanied by small i_0 values indicate that the electrochemical supply of electrons encounter a faradaic barrier and is slowed down quickly and the DL takes charge of the supply of energy at the specified power. The crossing of the Ragone plots at the low energy (high power density) region is in accord with the data presented in Figs. 4 and 5. The dependencies of dimensionless faradaic and DL discharge currents on the cell current and the exchange current density have been presented in Fig. 7a,b in three-dimensional plots. The behaviour in the region of low i_0 and low i_{cell} is interesting, where the two currents run in clear opposite directions. Although the low intrinsic rate of the supply of electron simply disables the faradaic contribution, the DL capacitor contribution takes charge pointing to the principal correct predictive capability of the model. The slowly rising DL contribution of current with the i_0 and i_{cell} is interesting. With increasing i_{cell} and at high i_0 values, the porous high area fails to deliver the current as the materials in the pores are depleted, and thus, the contribution of the DL discharge increases. This effect is certainly much smaller than the faradic part as what comparing Fig. 7a,b signifies. Figure 8 is a three-dimensional representative of the variation of θ with respect to i_{cell} and i_0. For small i_{cell} values, the cell remains in a charged state, and there is virtually no dependency of θ and i_0 as expected. Also, the changes of θ with i_{cell} at very low values of i_0 is marginal, as virtually no faradaic discharge takes place at the extreme lower end of i_{cell} and all the current is supplied by DL discharge. The steepest charge occurs along the bisectional plane of i_{cell}–i_0 angle where intrinsically fast kinetic capability accompanied by large drawn current tends to diminish θ to low values.

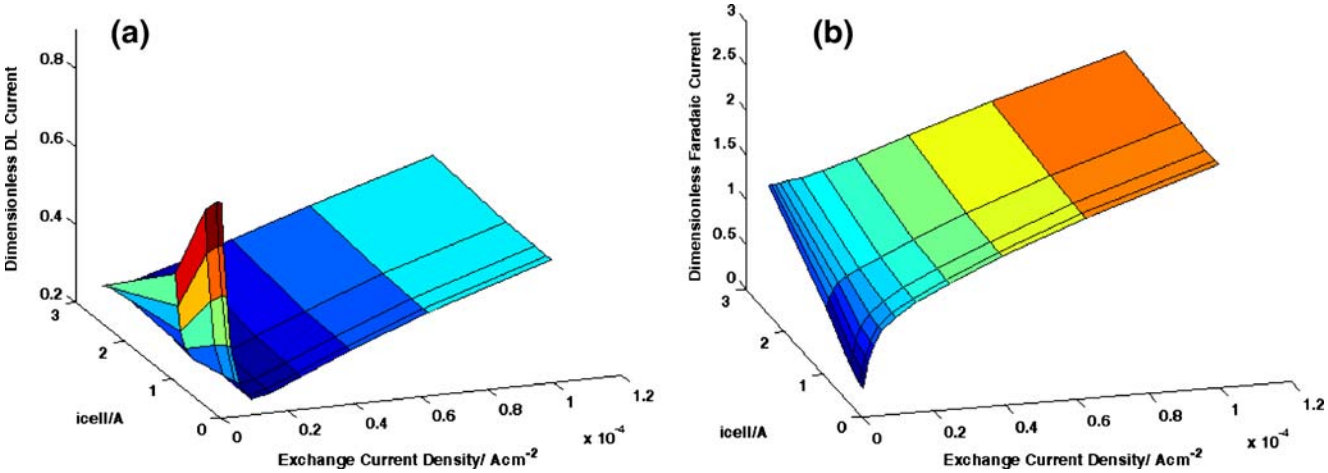

Fig. 7 Dependency of DL and faradaic currents to i_{cell} and exchange current density for simulated electrodes having 5-nm nano-particles and h=0.4 nm

Conclusion

The simulation of the discharge characteristics of a model capacitor comprising of DL and faradaic supercapacitors are carried out using basic principles. The discharge behaviour of the system is simulated, and the effects of a number of variables, exchange current density and unit cell length are considered. It is concluded that the model is well capable of simulating the behaviour and correctly predicting the trends. The contribution of two capacitors under various states of discharge are predicted and rationalized. The compensating contribution of the two contributors is concluded on the basis of discharge and Ragone plots.

References

1. Conway BE (1999) Electrochemical supercapacitors: Scientific fundamentals and technological applications. Kluwer, New York
2. Rodatz P, Paganelli G, Scicarretta A, Guzzella L (2005) Control Eng Pract 13:41
3. Kötz R, Carlon M (2000) Electrochim Acta 45:2483
4. Conway BE, Briss V, Wojtowicz J (1997) J Power Sources 66:1
5. Shi H (1996) Electrochim Acta 41:1633
6. Zheng JP, Cygan PJ, Jow TR (1995) J Electrochem Soc 142:2699
7. Jow TR, Zheng JP (1998) J Electrochem Soc 145:49
8. Liu KC, Anderson MA (1996) J Electrochem Soc 143:124
9. Wang YG, Xia YY (2006) Electrochim Acta 51:3223
10. Lin C, Ritter JA, Popov BN (1998) J Electrochem Soc 145:4097
11. Nagarajan N, Humadi H, Zhitomirsky I (2006) Electrochim Acta 51:3039
12. Lin C, Ritter JA, Popov BN, White RE (1999) J Electrochem Soc 146:3168
13. Lin C, Popov BN, Ploehn HJ (2000) J Electrochem Soc 149:A167
14. Christen T, Carlen MW (2000) J Power Sources 91:210
15. Christen T, Ohler C (2002) J Power Sources 110:107
16. Farsi H, Gobal F (2006) Artificial neural network simulator for supercapacitor performance prediction. Comput Mater Sci. DOI 10.1016/j.commatsci.2006.08.024
17. Pollak FH, O'Grady WE (1985) J Electrochem Soc 132:2385
18. Trasatti S, Lodi G (1980) Properties of conductive transition metal oxides with rutile-type structure. In: Trasatti S (ed) Electrodes of conductive metallic oxides—part A. Elsevier, New York, pp 301–358
19. Newman J, Thomas-Alyea KE (2004) Electrochemical systems. Wiley, New Jersey
20. Srinivasan V, Lin C, Ritter JA, Weidner JW (1996) Mathematical modeling of sol-gel derived carbon xerogels as double layer capacitors. In: Delnick FM, Ingersoll D, Andrieu X, Naoi K (eds) Electrochemical capacitors II, the Electrochemical Society proceedings series. Pennington, New Jersey, pp 153–166
21. Doubova LM, Daolio S, Battisti AD (2002) J Electroanal Chem 532:25
22. Subramanian VR, Devan S, White RE (2004) J Power Sources 135:361
23. Pell WG, Conway BE (1996) J Power Sources 63:255